Thermal Stability of Band Offsets of NiO/β-GaN

Xinyi Xia[1], Jian-Sian Li[1], Chao-Ching Chiang[1], Timothy Jinsoo Yoo[2], Fan Ren[1], Honggyu Kim[2] and S.J. Pearton[2]

[1] Department of Chemical Engineering, University of Florida, Gainesville, FL 32606 USA

[2] Department of Materials Science and Engineering, University of Florida, Gainesville, FL 32606 USA

ABSTRACT

NiO is a promising alternative to p-GaN as a hole injection layer for normally-off lateral transistors or low on-resistance vertical heterojunction rectifiers. The valence band offsets of sputtered NiO on c-plane, vertical geometry homoepitaxial GaN structures was measured by X-ray Photoelectron Spectroscopy as a function of annealing temperatures to 600°C. This allowed determination of the band alignment from the measured bandgap of NiO. This alignment was type II, staggered gap for both as-deposited and annealed samples. For the as-deposited heterojunction, ΔE_V=2.89 eV and ΔE_C= -2.39 eV, while for all the annealed samples the ΔE_V values were in the range 3.2-3.4 eV and ΔE_C values were in the range –(2.87-3.05) eV. The bandgap of the NiO was reduced from 3.90 eV as-deposited to 3.72 eV after 600°C annealing, which accounts for much of the absolute change in ΔE_V-ΔE_C. At least some of the spread in reported band offsets for the NiO/GaN system may arise from differences in their thermal history.

Keywords: Ga_2O_3, band offsets, heterojunctions, wide bandgap semiconductor

1. Introduction

There is considerable recent interest in developing GaN-based high efficiency power converters with much lower switching losses than Si devices [1-12]. GaN homostructures or AlGaN/GaN heterostructures also allow devices with smaller surface area and higher operating frequencies than Si. In addition, there can also be a reduction in the size of the associated parasitic inductors and capacitors, which lead to miniaturized, ultra-high-density power converters [1-12] and terahertz frequency multipliers [13]. GaN power devices are already commercialized for applications such as fast chargers, electric vehicles, data centers, and aerospace. The Huang Material figure-of-merit, $E_C\mu^{0.5}$, is a reliable predictor of power density in a variety of power converter types, where E_C is the critical electric field for breakdown and μ is the electron mobility [1-3]. Since E_C scales approximately as $E_G^{2.7}$, where E_G is the bandgap, more than an order of magnitude improvement in power density is enabled by use of GaN compared to Si [14-17]. GaN also has numerous advantages for power amplifiers and high-power switch technology for 5G-Advanced and 6G communications and base station radios, while reducing the system size and weight. A relatively new application is power electronics for electrified aircraft. The specific power of power electronics inverters for aircraft applications is approaching 20 kW/kg, and the peak efficiency can be above 99% [18,19].

One drawback is the relatively low hole concentrations obtainable in p-GaN, needed to provide p-gates in normally-off (enhancement mode) lateral transistors, which are more advantageous for power applications [14], or the p-side of vertical pin diodes. Recently, several reports have appeared on replacing p-GaN with p-type NiO [20-22]. This demonstrates higher hole concentration with similar work function to p-GaN and has been used to demonstrate normally off p-NiO gated AlGaN/GaN High Electron Mobility Transistors (HEMTs) [22]. Another

potential advantage is added flexibility in designing junction termination extension and p-type guard rings, as well as the fact that p-n junctions can readily afford avalanche breakdown, a key capability in many applications [23-28]. Normally-off devices require the application of a positive voltage to the gate to turn the device on [1,2]. Another common way to achieve a normally-off device is by tuning the AlGaN/GaN polarization to modulate the 2DEG by changing the doping or thickness of the AlGaN layer [1-7]. Commercial GaN normally-off devices are based either on the cascode or the p-GaN technology [1-3]. NiO has also been used as a hole injection layer on ZnO [29-32] and Ga_2O_3 heterojunction devices [33-44].

A key aspect in the performance of NiO/GaN devices is the thermal stability of the band alignment of the heterojunction. Gou et al.[9] reported there was interfacial reconstruction of the p-NiO/AlGaN interface and an increase in interface states due to formation of a thin c-Al_2O_3 insulating layer after 500 °C annealing. This change in the conduction-band profile at the interface produced a significant change in device operation characteristics. The valence band offset at the NiO/AlGaN interface was 1.64 eV prior to annealing and 1.86 eV after 500°C annealing. The band alignment was staggered type-II in both the initial and annealed NiO/AlGaN interfaces. Similar studies have been reported by several groups for NiO on pure GaN, with a significant spread in the respective band offsets [45-47].

. If NiO is to be useful as a hole injection layer on GaN, then the thermal stability of NiO/GaN heterointerfaces needs to be established so that the processing sequence can be optimized. In this paper we report measurements of the band alignment as a function of post-deposition annealing temperature up to 600°C and see a monotonic increase in the values of the staggered band offsets with annealing temperature.

2. Experimental

We used vertical rectifier structures for the measurement of band alignments. These were purchased from Kyma Technologies and consisted of a 8 μm thick, nominally undoped epitaxial layer grown by hydride vapor phase epitaxy (HVPE) with carrier concentration $5x10^{15}$ cm^{-3} on a c-plane, Si-doped n^+-GaN substrate. NiO layers were deposited by radio-frequency (RF) magnetron sputtering at <100°C temperature. The RF power was 150 W, and the purity of the dual NiO targets was 99.99%. During deposition, the chamber pressure was 3mTorr in an Ar/O_2 mixed ambient and the deposition rate was 0.2 $Å.sec^{-1}$. The Ar/O_2 ratio was used to control the doping in the NiO at ~10^{19} cm^{-3}, with mobility < 1 $cm^2 \cdot V^{-1} s^{-1}$. These values are consistent with literature values [48]. Three different types of sample were prepared, namely a thick layer (60 nm) of the NiO deposited on quartz, the bare GaN samples and a heterostructure consisting of a thin 5-10 nm) NiO layer on the GaN. A cross-sectional high-angle annular dark field (HAADF) scanning transmission electron microscope (STEM) image of the latter is shown in Figure 1. Given that HAADF-STEM images exhibit atomic weight sensitivity, the dark contrast at the interface of NiO and GaN is likely due to sputtering-induced disorder during deposition of the NiO. The interface itself is atomically abrupt with no extended defects into the substrate or film.

The TEM sample was fabricated along the $[21\bar{1}0]$ zone axis with a FEI Helios Dualbeam Nanolab 600 focused ion beam (FIB) system. HAADF-STEM imaging was performed on the aberration-corrected Themis Z (Fisher Scientific) at 200 kV with 30pA screen current.

The band gaps of NiO for as-deposited films and those after annealing at different temperatures were obtained using UV-Vis (Perkin-Elmer Lambda 800 UV/Vis spectrometer) absorbance spectrum. Tauc plots were used to calculate the bandgap of the NiO.

The band alignments were obtained using X-Ray Photoelectron Spectroscopy (XPS) [49] . The XPS system was a Physical Instruments ULVAC PHI, with an Al x-ray source (energy

1486.6 eV, source power 300W), analysis size of 100 μm diameter, a take-off angle of 50° and acceptance angle of ±7 degrees. The electron pass energy was 23.5 eV for high-resolution scans and 93.5 eV for survey scans. The total energy resolution of this XPS system is about 0.5 eV, and the accuracy of the observed binding energy is within 0.03 eV. The core levels and valence band maxima (VBM) positions were measured from the thick NiO layers and in the epitaxial GaN. These same core levels were re-measured in the NiO/GaN heterojunction. The acquired XPS spectra were calibrated using the C 1s peak at 284.8 eV are while this is not always reliable for calibration [50], any charging effect/band bending effect causes the peak shift by the same amout of energy [51]. This absolute binding energy is therefore not important in measuring the band structure. We subtracted the BE of Ga 2*p* and Ni 2*p* to eliminate possible charging effects on the band bending but in any case sample charging was not an issue in these conducting samples and was not observed.

The shift of the core level binding energy locations (ΔECL) within the heterostructure determines the valence band offset (ΔE_V) from [49, 52,53]

$$\Delta E_V = \Delta \text{ ECL} + (E_{Core} - E_{VBM})_{Ref.\ GaN} - (E_{Core} - E_{VBM})_{Ref.\ NiO}$$

The associated conduction band offsets, ΔE_C, were obtained by subtracting the valence band offsets from the bandgaps of the NiO and GaN.

3. Results and Discussion

The bandgaps of NiO were measured before and after annealing for 5 min at 300-600°C under an O_2 ambient. The bandgaps extracted from the Tauc plots were 3.90 eV (as-deposited), 3.84 eV (300°C), 3.76 eV (400°C), 3.74eV (500°C) and 3.72 eV(600°C). The as-deposited value is consistent with the range of values reported in the literature [48]. The small changes with annealing are also consistent with the literature [48].

The high resolution XPS spectra for the vacuum-core delta regions of GaN are shown in Figure 2 for as-deposited samples and those annealed at 300- 600°C. High resolution XPS spectra for the vacuum-core delta region of reference GaN sample are shown in Figure 3. The ΔE_V values are obtained from the shift of the core levels for the NiO/GaN heterojunction samples [49, 52,53]. The XPS spectra from which we extracted the core energy differences to VBM for thick NiO layers after different annealing temperatures are shown in Figure 4 and the peak position data summarized in Table 1. The corresponding valence band offsets were ΔE_V = 2.39 eV (as-deposited), 2.87 eV (300°C), 2.87 eV(400°C), 3.05 eV(500°C) and 2.88 eV(600°C). The respective conduction band offsets are then -2.89 eV (as-deposited), -3.31 eV (300°C), -3.23 eV (400°C), -3.39 eV (500°C) and -3.2 eV (600°C).The error bars were ±.025 eV for all these values. [52,53].

Figure 5 shows the annealing temperature dependence of the band alignment of NiO on GaN. The band alignment is staggered, type II in all cases. The band offsets increase monotonically with annealing temperature and will not provide any barrier to either electrons or holes moving into the GaN. Gong et al. [9] reported a similar trend for NiO on $Al_{0.25}Ga_{0.75}N$, with a type II alignment, valence band offset of 1.64 eV and conduction band offset of 1.37 eV for the as-deposited case and observing an increase in these values to ΔE_V=1.86 eV and ΔE_C=1.63 eV after annealing at 500°C. This was speculated to be due to O atom incorporation replacing N sites at the NiO/AlGaN interface and also the formation of a thin Al_2O_3 layer [9]. The latter is obviously absent in our samples, which do not include AlGaN. Zhang et al.[45] reported valence and conduction band offsets of 1.63 eV and 1.38 eV, respectively, for reactively sputtered NiO on AlGaN/GaN heterostructures. The deposition temperature was below 30°C in this case [45]. Baraik et al.[46] determined ΔE_V and ΔE_C values of 1.4 and 1.9 eV for NiO/GaN where the NiO

was deposited by pulsed laser deposition at 600°C, while Li et al.[47] presented the VBO and CBO values of 1.2 and 1.5 eV for NiO/GaN where the NiO was formed by oxidation of Ni at 500°C. These results are summarized in Table II, which emphasizes the large spread in reported values. However, all of them agree on the type of alignment. Figure 5 appears to show an apparent saturation of the change in magnitude of band offsets, at least up to 600°C. Given that Ohmic contact annealing temperatures for GaN are much higher than this temperature, the NiO would need to be deposited after the Ohmic contact formation. It is also noteworthy from the literature that the higher deposition temperatures produce band offsets values closest to our values after annealing.

The large variation in deposition or formation temperatures for the NiO in previous work may explain the spread in reported values of valence and conduction band offsets. Hays et al.[53] summarized possible reasons for variations in band offsets between nominally similar systems, including different strain, interfacial disorder and contamination, stoichiometry and chemical bonding variations. At this stage, the exact cause cannot be isolated and awaits more experiments where deposition conditions are carefully controlled.

4. Conclusions

The spread in reported values for the valence band offsets, which vary from 1.2-2.39 and conduction band offsets, which vary from –(1.3-2.89) eV show there is still additional work that to understand the NiO/GaN interface and its variability with deposition method, thermal budget and surface cleaning procedure. The reported variations in reported band offsets in this system requires examination of less energetic deposition methods than sputtering, since disruption to the interfacial region is known to affect band alignment.

5. Conflicts of interest

There are no competing financial interests in this paper.

6. Data Availability

All data that support the findings of this study are included within the article.

7. Acknowledgments

The work at UF was performed as part of Interaction of Ionizing Radiation with Matter University Research Alliance (IIRM-URA), sponsored by the Department of the Defense, Defense Threat Reduction Agency under award HDTRA1-20-2-0002. The content of the information does not necessarily reflect the position or the policy of the federal government, and no official endorsement should be inferred. The work at UF was also supported by NSF DMR 1856662 (James Edgar).

References

1. Houqiang Fu, Kai Fu, Chen Yang, Hanxiao Liu, Kevin A. Hatch, Prudhvi Peri, Dinusha Herath Mudiyanselage, Bingjun Li, Tae-Hyeon Kim, Shanthan R. Alugubelli, Po-Yi Su, Daniel C. Messina, Xuguang Deng, Chi-Yin Cheng, Reza Vatan Meidanshahi, Xuanqi Huang, Hong Chen, Tsung-Han Yang, Jingan Zhou, Andrew M. Armstrong, Andrew A. Allerman, Edward T. Yu, Jung Han, Stephen M. Goodnick, David J. Smith, Robert J. Nemanich, Fernando A. Ponce, Yuji Zhao, Mater. Today (2021).

2. Matteo Meneghini, Carlo De Santi, Idriss Abid, Matteo Buffolo, Marcello Cioni, Riyaz Abdul Khadar, Luca Nela, Nicolò Zagni, Alessandro Chini, Farid Medjdoub, Gaudenzio Meneghesso, Giovanni Verzellesi, Enrico Zanoni, and Elison Matioli, J. Appl. Phys. 130, 181101 (2021).

3. Houqiang Fu, Kai Fu, Srabanti Chowdhury, Tomás Palacios and Yuji Zhao, IEEE T Electron Dev., 68, 3200 (2021)

4. Taofei Pu, Usman Younis, Hsien-Chin Chiu, Ke Xu, Hao-Chung Kuo and Xinke Liu, Nanoscale Res Lett 16, 101 (2021).

5. Y. Zhang, A. Dadgar and T. Palacios J. Phys D Appl Phys., 51, 273001(2018)

6. M.A. Ebrish, M. Porter, A.G. Jacobs, J.C. Gallagher, R.J. Kaplar, B.P. Gunning, K.D. Hobart and T.J. Anderson, Crystals, 12, 623 (2022).

7. X. Liu,Q. Liu, C. Li, J. Wang, W. Yu, K. Xu and J.P. Ao, Jpn J Appl Phys 56, 026501 (2017).

8. T. Oka, Jpn J. Appl Phys 58, SB0805 (2019).

9. Hui Guo, Hehe Gong, Xinxin Yu, Rui Wang, Qing Cai, Junjun Xue, Jin Wang, Danfeng Pan, Jiandong Ye, Bin Liu, Dunjun Chen, Hai Lu, Rong Zhang, and Youdou Zheng, Appl. Phys. Rev. 8, 041405 (2021).

10. Y. Sun, X. Kang, Y. Zheng, J. Lu, X. Tian, K. Wei, H. Wu, W. Wang, X. Liu and G. Zhang, Electronics 8, 575 (2019).

11. H Amano, Y Baines, E Beam, Matteo Borga, T Bouchet, Paul R Chalker, M Charles, Kevin J. Chen, Nadim Chowdhury, Rongming Chu, Carlo De Santi, Maria Merlyne De Souza, Stefaan Decoutere, L Di Cioccio, Bernd Eckardt, Takashi Egawa, P. Fay, Joseph J. Freedsman, L. Guido, Oliver Häberlen, Geoff Haynes, Thomas Heckel, Dilini Hemakumara, Peter Houston, Jie Hu, Mengyuan Hua, Qingyun Huang, Alex Huang, Sheng Jiang, H Kawai, Dan Kinzer, Martin Kuball, Ashwani Kumar, Kean Boon Lee, Xu Li, Denis Marcon, Martin März, R McCarthy, Gaudenzio Meneghesso, Matteo Meneghini, E Morvan, A Nakajima, E M S Narayanan, Stephen Oliver, Tomás Palacios, Daniel Piedra, M. Plissonnier, R. Reddy, Min Sun, Iain Thayne, A Torres, Nicola Trivellin, V. Unni, Michael J. Uren, Marleen Van Hove, David J Wallis, J .Wang, J. Xie, S. Yagi, Shu Yang, C Youtsey, Ruiyang Yu, Enrico Zanoni, Stefan Zeltner and Yuhao Zhang, J. Phys D. Appl Phys 51, 163001 (2018).

12. R. Xu, P. Chen, M. Liu, J. Zhou, Y. Yang, Y. Li, C. Ge, H. Peng, B. Liu, D. Chen, Z. Xie, R. Zhang, Y .Zheng, IEEE J Electron Devi, 8, 316 (2020).

13. S. Liang, Xubo Song, Lisen Zhang, Yuanjie Lv, Yuangang Wang, Bihua Wei, Yanmin Guo, Guodong Gu, Bo Wang, Shujun Cai and Zhihong Feng, IEEE Electr Device L. 41, 669 (2020).

14. Y. Uemoto, M. Hikita, H. Ueno, H. Matsuo, H. Ishida, M. Yanagihara, T. Ueda, T. Tanaka, and D. Ueda, IEEE T Electr Dev 54, 3393 (2007).

15. Luke Yates, Brendan P Gunning, Mary H Crawford, Jeffrey Steinfeldt, Michael L Smith, Vincent M Abate, Jeramy R Dickerson, Andrew M Armstrong, Andrew Binder, Andrew A Allerman and Robert J. Kaplar, IEEE T. Electron Dev.69, 1931 (2022).

16. Man Hoi Wong, Oliver Bierwagen, Robert J. Kaplar and Hitoshi Umezawa, J. Mater. Res. 36,4601 (2021).

17. Robert J. Kaplar, Oleksiy Slobodyan, Jack D Flicker and Mark A Hollis, ECS Meeting Abstracts, 31, 1334 (2019) (IOP Publishing, 2019).

18. A. Barzkar and M. Ghassemi, IEEE Access, 8, 169314 (2020).

19. Z. Dong, R. Ren, and F. Wang, IEEE J. Emerg. Sel. Topics Power Electron., early access, 2022, doi: 10.1109/JESTPE.2021.3139903.

20. G. J. Li, X. M. Li, J. L. Zhao, F. W. Yan, Q. X. Zhu, and X. D. Gao, J. Mater. Chem. C 8, 1125 (2020).

21. L. A. Li, J. Chen, Z. X. Liu, T. T. Que, X. Gu, L. He, and Y. Liu, Appl. Surf. Sci. 475, 1043 (2019).

22. Y. Ren, L. A. Li, N. Y. Liu, K. Zhang, C. G. Li, Z. T. Chen, and B. J. Zhang, Vacuum 182, 109784 (2020).

23. J.S. Lee, J.D. Lim, Z.G. Khim, Y.D. Park, S.J. Pearton, S.N.G. Chu, J. Appl. Phys. 93, 4512 (2003).

24. K. Nie, W. Xu, F. Ren, D. Zhou, D. Pan, J. Ye, D. Chen, R. Zhang, Y. Zheng and H .Lu, IEEE Electr Device L. 41, 469 (2020).

25. X. Li, T. Pu, T. Zhang, X. Li, L. Li and J.P. Ao, IEEE Sens. J. 20, 62 (2020).

26. Y. Wang, T. Pu, X. Li, L. Li and J.P. Ao, Mater. Sci. Semicond. Proc 125, 105628 (2021)

27. J. Zhou, L. He, X. Li, T. Pu, L. Li and J.P. Ao, Superlattice Microst 151, 106820 (2021).

28. L. Li , X. Wang, Y. Liu and J.P. Ao, J. Vac Sci Technol A 34, 02D104 (2015).

29. T. D. Desissa, Ceram Int,47, 8053 (2021).

30. R.K. Gupta, K. Ghosh and P.K. Kahoi, Physica E Low-dimensional Systems and Nanostructures 41, 617 (2009).

31. P. K. Das, R. Biswal, R. J. Choudhary, S. A. Khan, R C Meena, N. C. Mishra and P. Mallick, Mater. Res. Express 6, 106413 (2019).

32. A. Merih Akyuzlu, F. Dagdelen, Fahrettin Yakuphanoglu, Ahmet Gultek and A. A. Hendi, Eur. Phys. J. Plus 132, 178 (2017)

33. Y. Kokubun, S. Kubo, S. Nakagomi, APEX, 9, 091101(2016).

34. Andrew J. Green, James Speck, Grace Xing, Peter Moens, Fredrik Allerstam, Krister Gumaelius, Thomas Neyer, Andrea Arias-Purdue, Vivek Mehrotra, Akito Kuramata, Kohei Sasaki, Shinya Watanabe, Kimiyoshi Koshi, John Blevins, Oliver Bierwagen, Sriram Krishnamoorthy, Kevin Leedy, Aaron R. Arehart, Adam T. Neal, Shin Mou, Steven A. Ringel, Avinash Kumar, Ankit Sharma, Krishnendu Ghosh, Uttam Singisetti, Wenshen Li, Kelson Chabak, Kyle Liddy, Ahmad Islam, Siddharth Rajan, Samuel Graham, Sukwon Choi, Zhe Cheng, and Masataka Higashiwaki, APL Mater. 10, 029201 (2022).

35. S. J. Pearton, Fan Ren, Marko Tadjer and Jihyun Kim, J. Appl. Phys. 124, 220901 (2018).

36. Chenlu Wang, Jincheng Zhang, Shengrui Xu, Chunfu Zhang, Qian Feng, Yachao Zhang, Jing Ning, Shenglei Zhao, Hong Zhou and Yue Hao, J. Phys. D: Appl. Phys. 54, 243001 (2021).

37. W. Xiong, X. Zhou, G. Xu, Q. He, G. Jian, C. Chen, Y. Yu, W. Hao, X. Xiang, X. Zhao, W. Mu, Z. Jia, X. Tao, and S. Long, IEEE Electr. Device L.42, 430 (2021).

38. Ming Xiao, Boyan Wang , Jingcun Liu , Ruizhe Zhang, Zichen Zhang, Chao Ding, Shengchang Lu, Kohei Sasaki, Guo-Quan Lu, Cyril Buttay, and Yuhao Zhang, IEEE T Power Electr. 36, 8565 (2021).

39. X. Lu, Xianda Zhou, Huaxing Jiang, Kar Wei Ng, Zimin Chen, Yanli Pei, Kei May Lau and Gang Wang, IEEE Electr. Device L.41, 449 (2020).

40. Qinglong Yan, Hehe Gong, Jincheng Zhang, Jiandong Ye, Hong Zhou, Zhihong Liu, Shengrui Xu, Chenlu Wang, Zhuang Hu, Qian Feng, Jing Ning, Chunfu Zhang, Peijun Ma, Rong Zhang, and Yue Hao, Appl. Phys. Lett. 118, 122102 (2021).

41. H. H. Gong, X. X. Yu, Y. Xu, X. H. Chen, Y. Kuang, Y. J. Lv, Y. Yang, F.-F. Ren, Z. H. Feng, S. L. Gu, Y. D. Zheng, R. Zhang, and J. D. Ye, Appl. Phys. Lett. 118, 202102 (2021).

42. W. Hao, Q. He, K. Zhou, G. Xu, W. Xiong, X. Zhou, G. Jian, C. Chen, X. Zhao, and S. Long, Appl. Phys. Lett., 118, 043501 (2021).

43. F. Zhou, Hehe Gong, Weizong Xu, Xinxin Yu, Yang Xu, Yi Yang, Fang-fang Ren, Shulin Gu, Youdou Zheng, Rong Zhang, Jiandong Ye and Hai Lu, IEEE T Power Electr, 37, 1223 (2022).

44. Qinglong Yan, Hehe Gong, Hong Zhou, Jincheng Zhang, Jiandong Ye, Zhihong Liu, Chenlu Wang, Xuefeng Zheng, Rong Zhang, and Yue Hao, Appl. Phys. Lett. 120, 092106 (2022).

45. Tong Zhang, Lei Wang, Xiaobo Li, Yuyu Bu, Taofei Pu, Ruiling Wang, Liuan Li, Jin-Ping Ao, Appl. Surf. Sci, 462, 799 (2018).

46. K. Baraik, S.D. Singh, Y. Kumar, R.S. Ajimsha, P. Misra, S.N. Jha, T. Ganguli, Appl. Phys. Lett., 110, 191603 (2017).

47. L. Li, W. Wang, L. He, X. Zhang, Z. Wu, Y. Liu, J. Alloy. Compd., 728, 400 (2017).

48. J.A. Spencer, A.L. Mock, A.G. Jacobs, M. Schubert, Y. Zhang, M.J. Tadjer, Appl. Phys. Rev. 9, 011315 (2022).

49. E. A. Kraut, R. W. Grant, J. R. Waldrop, and S. P. Kowalczyk, Phys. Rev. Lett., 44, 1620 (1980).

50. G. Greczynsk and L. Hultman, Appl. Surf. Sci. 451, 99 (2018).

51. Z. Feng, Y. Peng, Y. Shen, Z. Li, H. Wang, X. Chen, Y. Wang, M. Jing, F. Lu, W Wang, Y. Cheng, Y. Cui, A. Dingsun, G. Han, H. Liu and H. Dong, , Adv. Electron. Mater., 7, 2100414 (2021).

52. C. Fares, F. Ren, Max Knessl, H. von Wenckstern, M. Grundmann and S.J. Pearton, chapter 9 in Wide Bandgap Semiconductor Based Electronics, ed F. Ren and S.J. Pearton (IOP Publishing, Bristol, (2020).

53. D. C. Hays, B.P. Gila, S. J. Pearton and F. Ren, Appl. Phys. Rev. 4, 021301 (2017).

.

Table I. Summary of measured core levels (eV) for NiO, and a heterostructure of NiO deposited on GaN as a function of post-deposition annealing temperature.

	Bulk NiO			**NiO/GaN heterojunction**		
Anneal T(°C)	**VBM**	**Core Level Peak (Ni 2p)**	**Core-VBM**	**Core Level Peak (Ga 3d)**	**Core Level Peak (Ni 2p)**	**△Core level**
As-deposited	-0.6	853.4	854.0	18.27	852.48	834.21
300	-1.8	853.2	855.0	17.72	852.45	834.73
400	-1.9	853.1	855.0	17.71	852.44	834.73
500	-1.9	853.4	855.3	17.7	852.55	834.85
600	-1.7	853.7	855.4	17.37	852.49	835.12

Table II. Reported values for band offsets of NiO on GaN or AlGaN

NiO deposition	**ΔEc (eV)**	**ΔE_V (eV)**	**Reference**
PLD, 600°C	-1.9	1.4	46
Reactive sputtering, RT	-1.38	1.63	45
E beam Ni, oxidation at 500°C	-1.5	1.2	47
*$Al_{0.25}Ga_{0.75}N$, rf magnetron, RT	-1.63	1.86	9
Magnetron sputtering	-2.34	2.89	This work

Figure Captions

Figure 1. Atomic-resolution HAADF-STEM images of the NiO/GaN heterojunction at two different magnifications. The GaN substrate remains fairly pristine (a) while the NiO film is polycrystalline and ~ 5nm in thickness. The interface is atomically abrupt, and the dark contrast is likely due to sputtering-induced disorder (b).

Figure 2.ΔCore level calculations for interfaces of thin NiO/GaN as-deposited and annealed at different temperatures from 300-600°C.

Figure 3. High resolution XPS spectra for the vacuum-core delta region of reference GaN sample.

Figure 4. Core-VBM calculations for thick NiO film as-deposited and annealed at different temperatures from 300-600°C.

Figure 5. Schematic of band alignments for NiO/GaN as a function of post-deposition annealing temperature from 300-600°C.

(a)

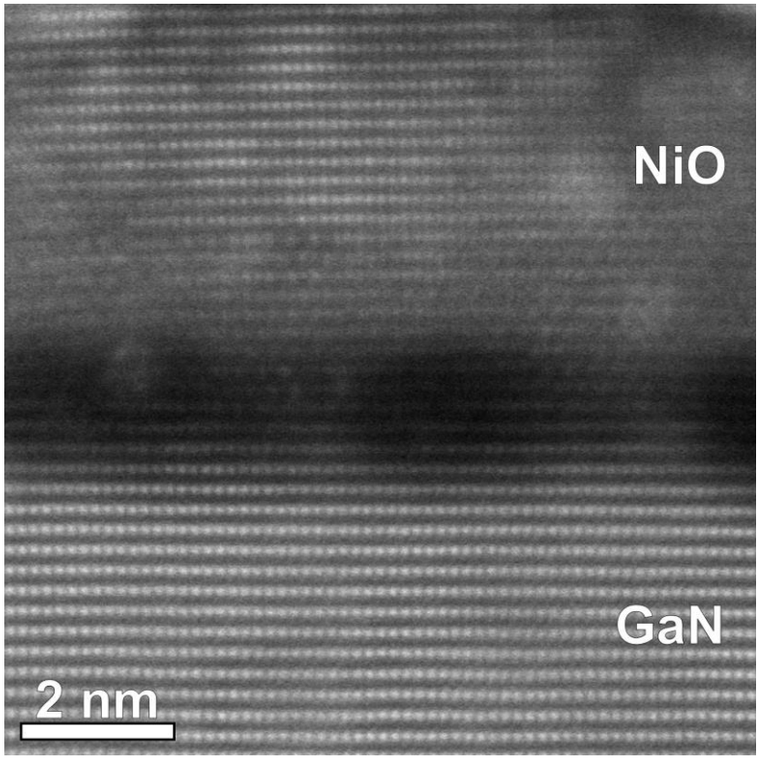

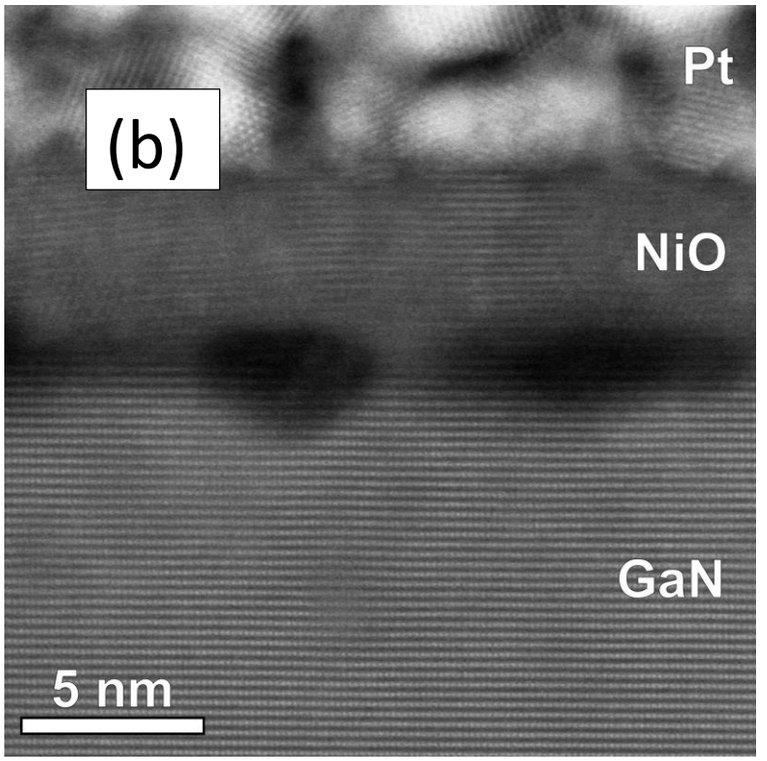

Journal of Vacuum Science Technology A

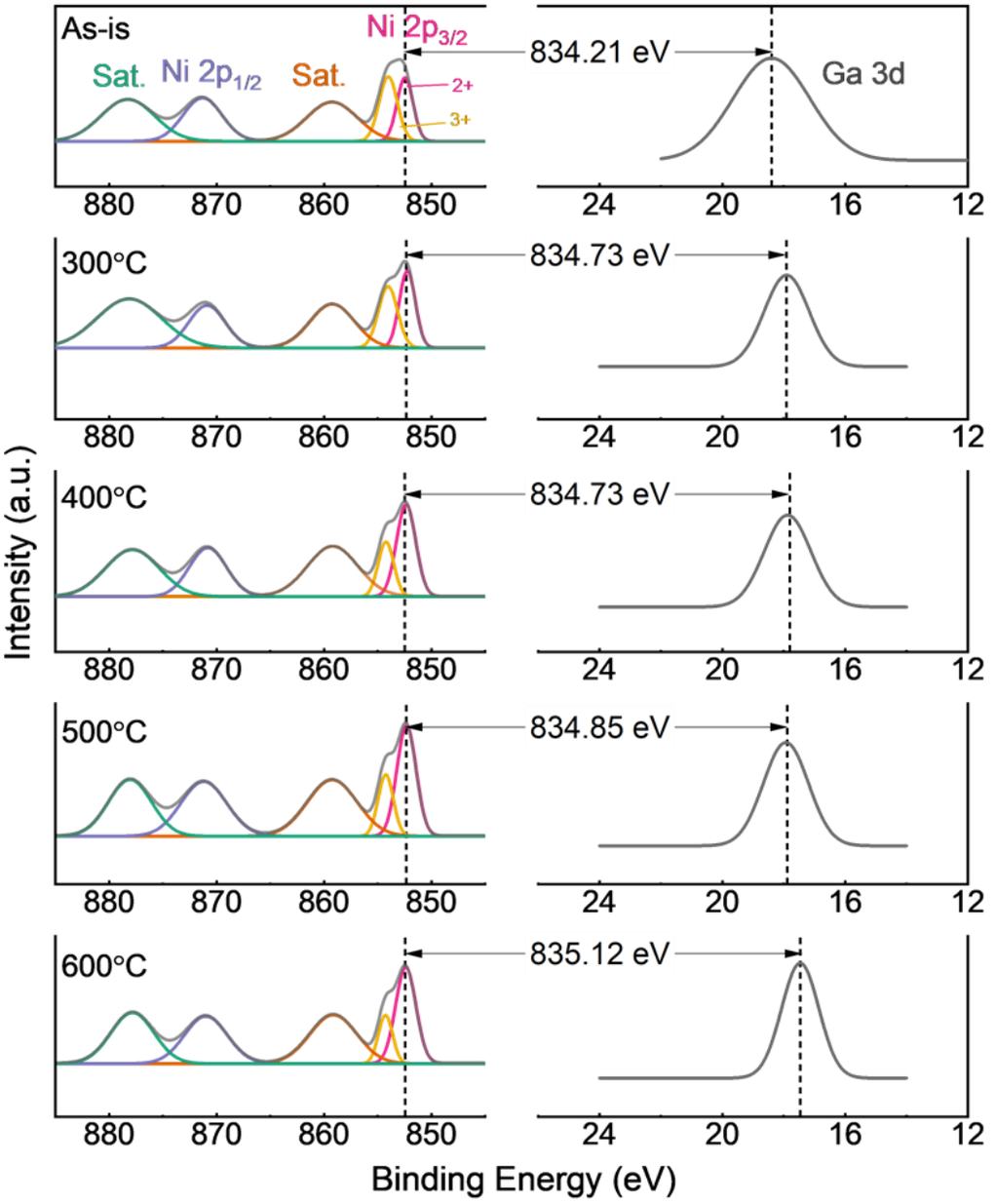

Journal of Vacuum Science Technology A

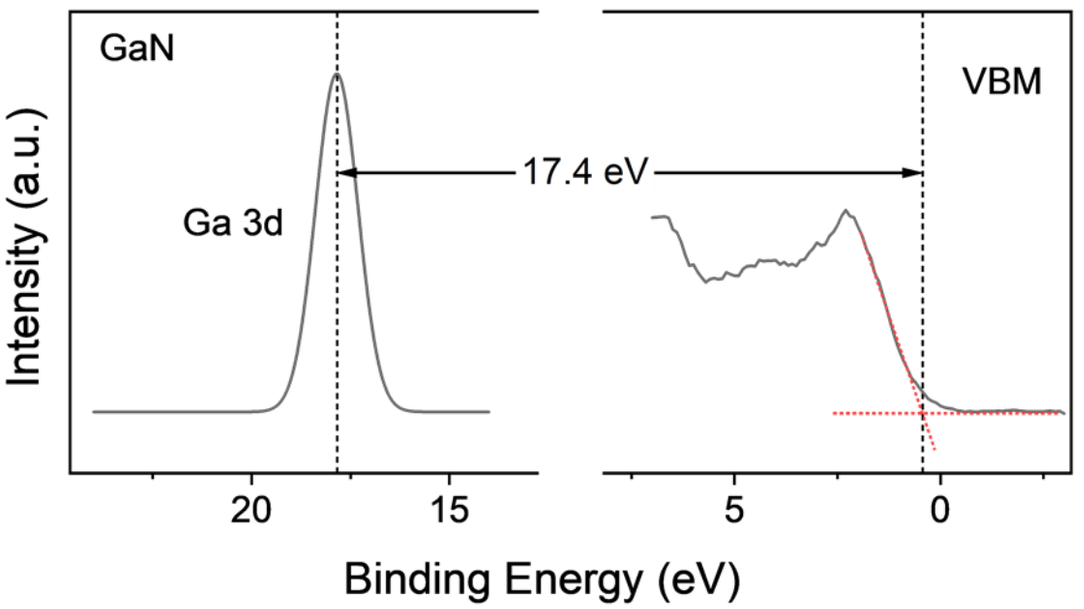

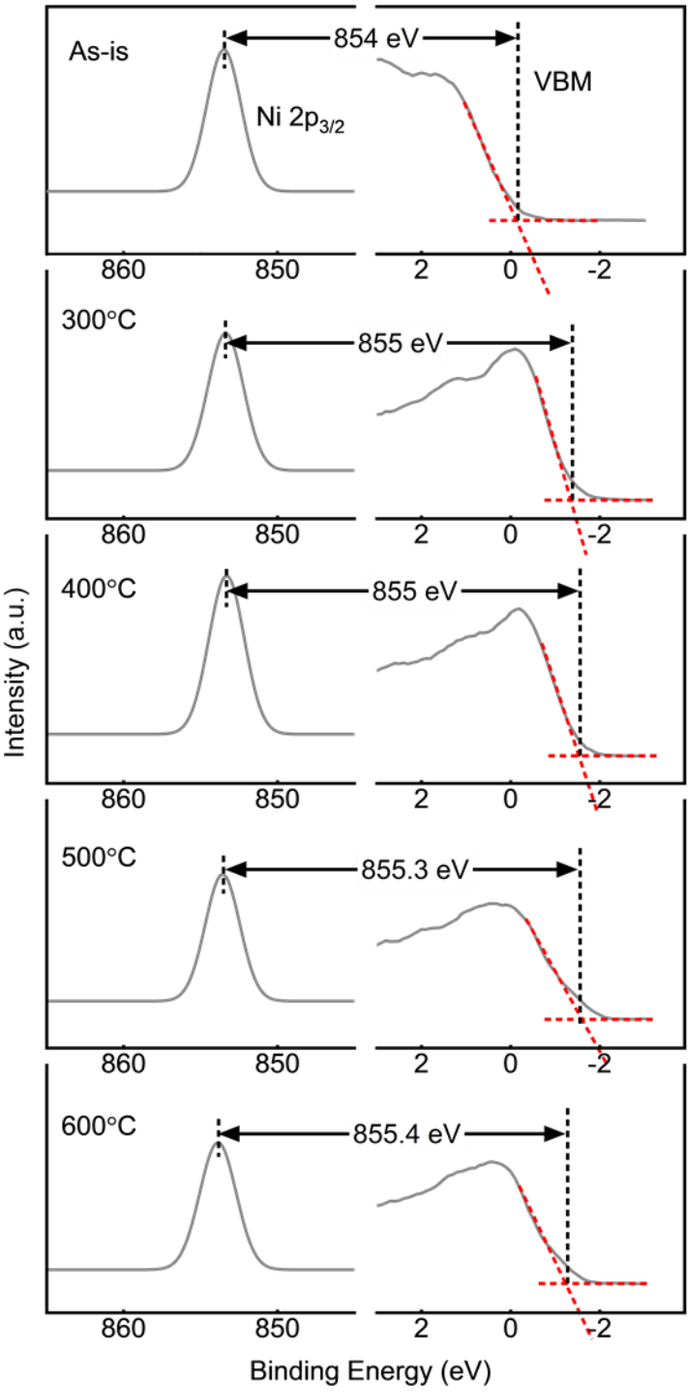

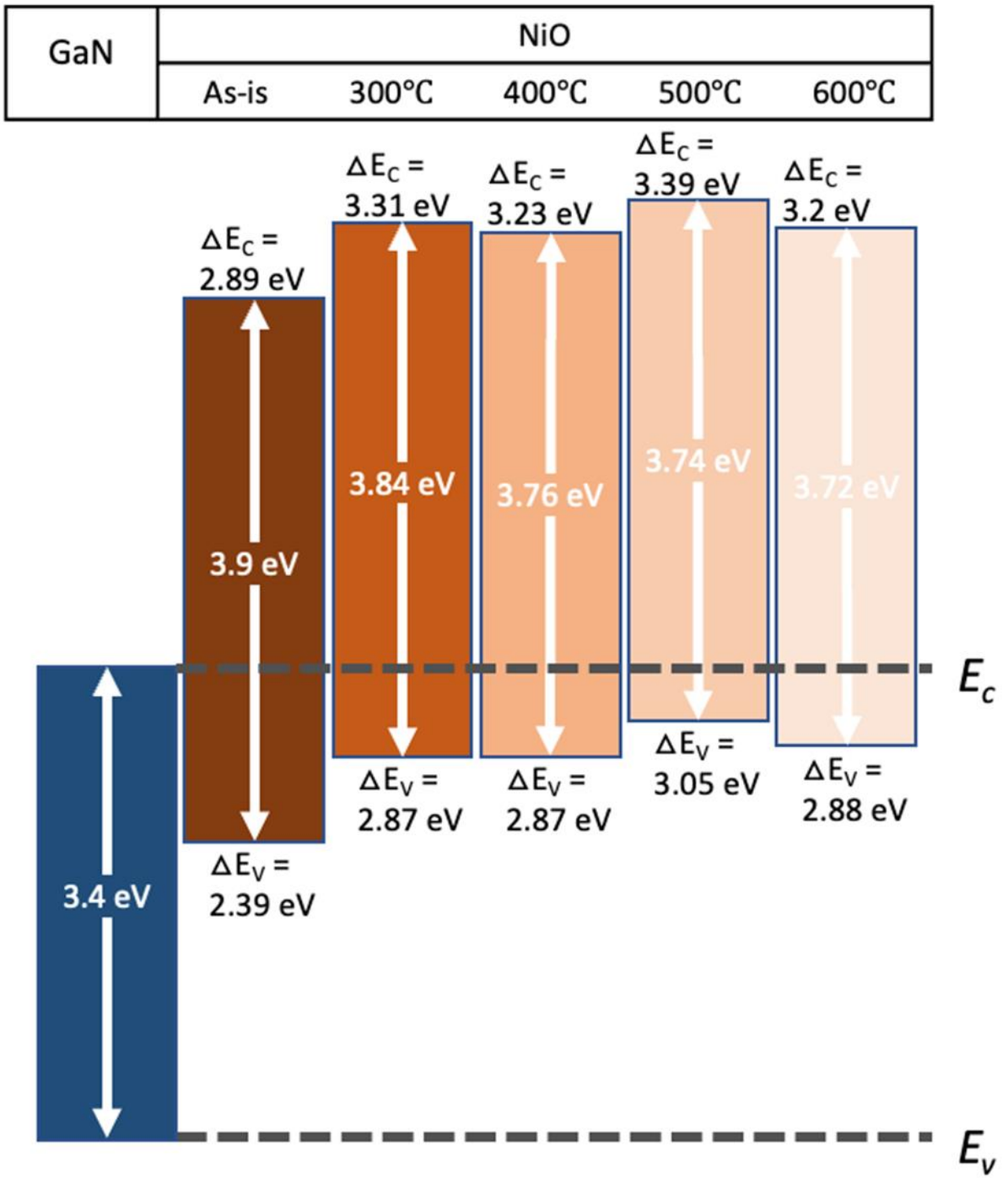

Journal of Vacuum Science Technology A

PLEASE CITE THIS ARTICLE AS DOI: 10.1116/6.0002033

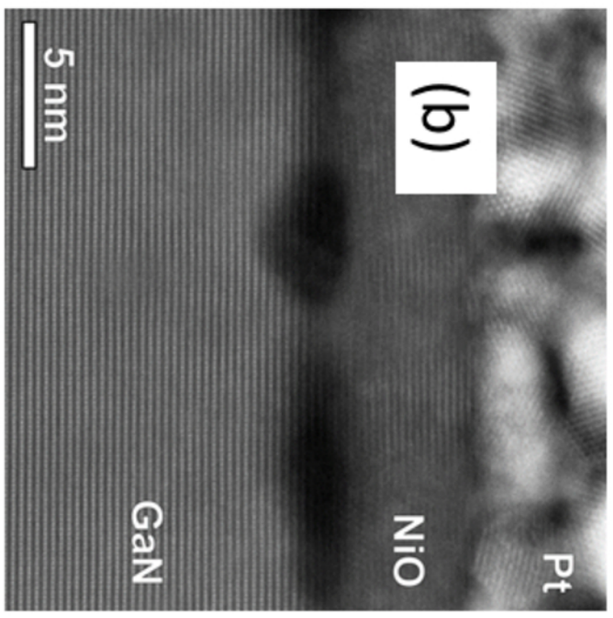

Journal of Vacuum Science Technology A

PLEASE CITE THIS ARTICLE AS DOI: 10.1116/6.0002033

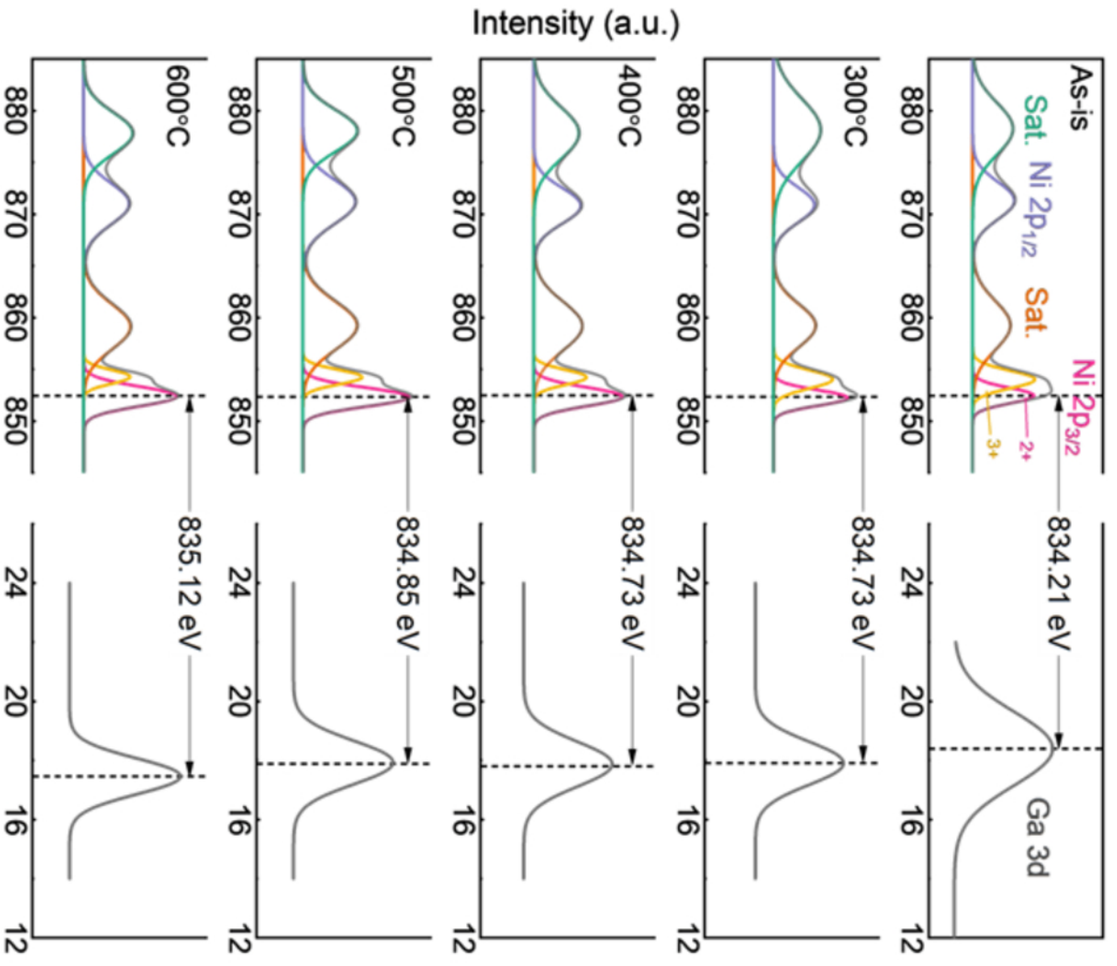

Journal of Vacuum Science Technology A

PLEASE CITE THIS ARTICLE AS DOI: 10.1116/6.0002033

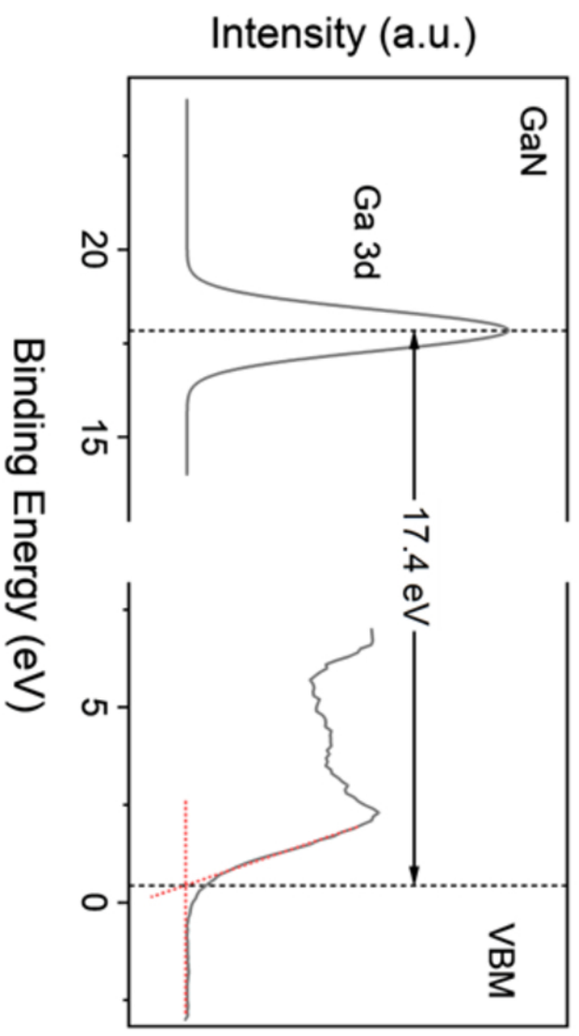

Journal of Vacuum Science Technology A

PLEASE CITE THIS ARTICLE AS DOI: 10.1116/6.0002033

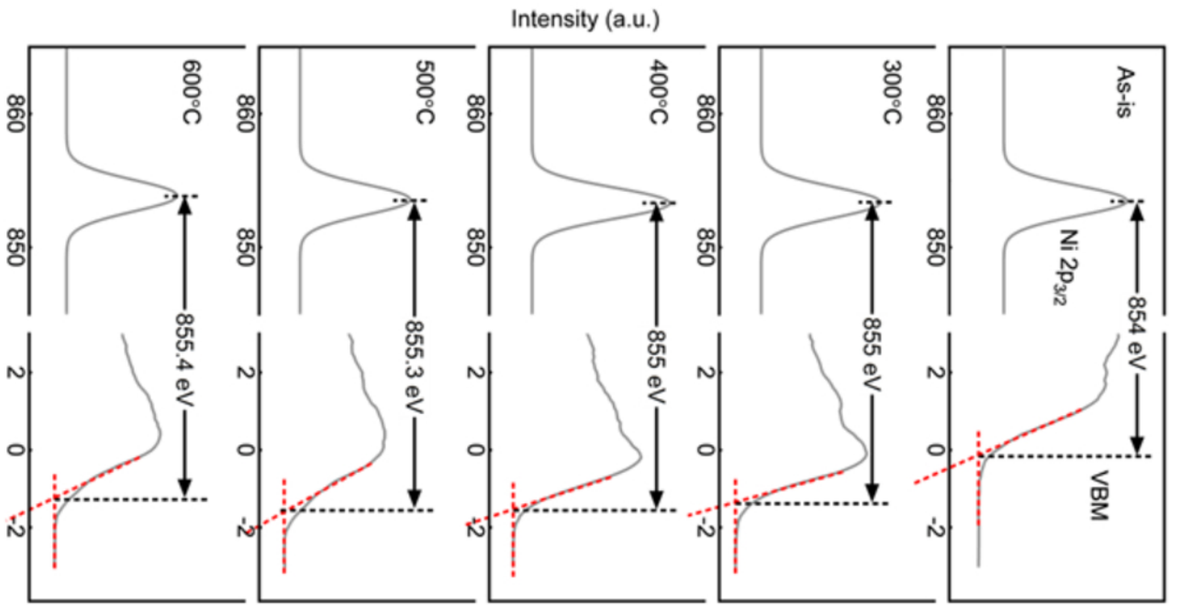

Journal of Vacuum Science Technology A